American Mineralogist, Volume 89, pages 1092–1100, 2004

Pyrophyllite dehydroxylation process by First Principles calculations

C. Ignacio Sainz-Díaz,* Elizabeth Escamilla-Roa, and Alfonso Hernández-Laguna

Department of Earth Sciences and Environmental Chemistry, Estación Experimental del Zaidín, Consejo Superior de Investigaciones Científicas, C/ Profesor Albareda 1, 18008, Granada, Spain

Abstract

The crystal structure of triclinic pyrophyllite and its dehydroxylate derivative was studied with quantum mechanical calculations. The standard Kohn-Sham self-consistent density functional theory (DFT) was used through a linear-scaling DFT method with periodical boundary conditions in the generalized gradient approximation (GGA) with numerical atomic orbitals as the basis set. The calculations reproduce the lattice parameters found experimentally in pyrophyllite and its dehydroxylate derivative. The geometrical disposition of the OH bond in the crystal lattice and the hydrogen bonds and other electrostatic interactions of this group were analyzed. The frequencies of different vibration modes were calculated and compared with experimental data; the results show a good agreement. The dehydroxylation process, including different intermediates of this reaction, was investigated theoretically. The energetic differences are according to the thermodynamics of the experimental process. The semidehydroxylate derivative is identified, for the first time, as an important intermediate in this process, clarifying previous questions concerning the mechanism reported from the experimental data.

Introduction

Pyrophyllite [$Si_8Al_4O_{20}(OH)_4$ per unit cell] is a dioctahedral 2:1 phyllosilicate in which a sheet of octahedrally coordinated Al cations is sandwiched between two sheets of linked silica tetrahedra. Two polytypes of pyrophyllite are found mixed in nature: one-layered triclinic (1*Tc*) and two-layered monoclinic (2*M*) (Wardle and Brindley 1972). This mineral is used widely in the manufacture of glass, ceramics, refractory materials, and pressure-transfer media. Knowledge of the stability of this mineral is important in evaluating its applications, given that stability failure under thermal treatment can produce mineral transformations or a dehydroxylation process and a change in the physical-chemical properties of the mineral. A better knowledge of the thermally induced degradation process of pyrophyllite could be very useful for some of its industrial applications.

The cations of the octahedral sheet are coordinated with six O atoms, two of which are in hydroxyl groups (Fig. 1a). The study of the structure and properties of these hydroxyl groups is interesting because they participate in the crystallographic and physical-chemical properties and stability of clay minerals (Heller et al. 1962; Emmerich et al. 1999; Drits et al. 1995; Wang et al. 2002). The dehydroxylation of pyrophyllite to pyrophyllite dehydroxylate involves the reaction of the two OH groups, yielding the formation and elimination of one water molecule per half unit cell. Previous studies involving infrared spectroscopy (Wang et al. 2002), Nuclear Magnetic Resonance (NMR) (Fitzgerald et al. 1996), and powder X-ray diffraction (XRD) (Wardle and Brindley 1972) showed that pyrophyllite dehydroxylate consists of five-coordinate, distorted, trigonal bipyramidal AlO_5 units in the octahedral sheet (Fig. 1b), sandwiched between two distorted but intact tetrahedral SiO_4 sheets (Fitzgerald et al. 1996; Wang et al. 2002). However, some aspects of the process of thermally induced dehydroxylation of pyrophyllite remain only partially understood. Thermogravimetric studies of this process showed that the release of water happens in a two-step process (Guggenheim et al. 1987). The temperature range of this process is very wide, from 450 to 850 °C. Recent spectroscopic studies of this process revealed the formation of an intermediate phase during the dehydroxylation of pyrophyllite, but no structure was proposed. Previous rehydroxylation studies reported that an intermediate phase should be formed during the rehydroxylation of the dehydroxylate pyrophyllite, but the identity of this intermediate remains unknown (Heller et al. 1962). One of the aims of this work is to study the crystal structure of pyrophyllite and the dehydroxylate derivative and to study the dehydroxylation process at a microscopic scale.

Atomistic calculations with empirical potentials have been applied to layered 2:1 phyllosilicates (Teppen et al. 1997; Sainz-Díaz et al. 2001a, 2001b) with good agreement with experimental structural data. However, the hydrogen bonding, the relatively weak interactions in the interlayer space, and the real total energy calculations require, as a minimum, the most sophisticated and exact methods provided by quantum mechanic theory. First-principles quantum techniques, based on density functional theory (DFT) with periodic boundary conditions, have been used in the study of layered phyllosilicates (Bridgeman et al. 1996; Bickmore et al. 2003; Hobbs et al. 1997; Sainz-Díaz et al. 2002) with good agreement with experimental data. The properties of the OH groups in pyrophyllite and smectites and illites have been studied previously by means of quantum mechanical research using cluster (Sainz-Díaz et al. 2000; Timón et al. 2003) and crystal lattice (Sainz-Díaz et al. 2002; Botella et al. 2004) models. Recently, First Principles calculations of the pyrophyllite crystal structure have been reported using pseudopotential plane-wave DFT methods (Bickmore et al. 2003; Refson et al. 2003; Stackhouse et al. 2001). However, the agreement with experimental geometrical features was not as good as for our

* E-mail: Sainz@eez.csic.es

0003-004X/04/0007–1092$05.00

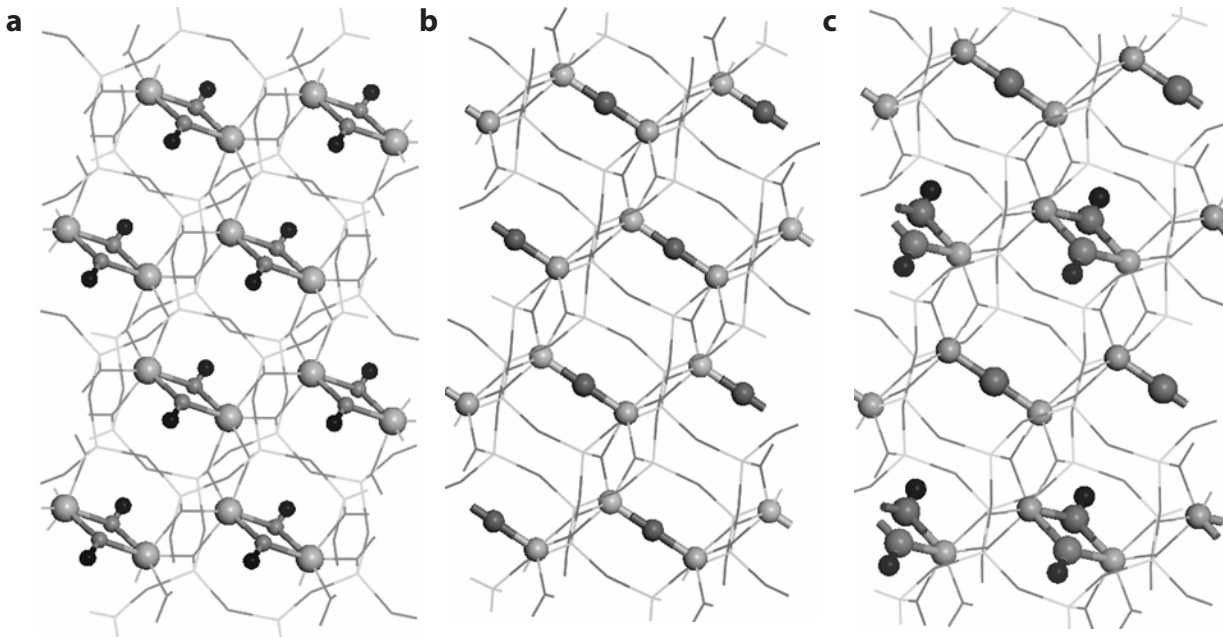

FIGURE 1. Optimized crystalline structures of pyrophyllite (**a**), dehydroxylate (**b**), and semidehydroxylate (**c** and **d**) derivatives. The H atoms, the O atoms of the OH groups, and the Al atoms are shown as black, dark grey, and light grey spheres, respectively. Views are from the 001 plane (**a**, **b**, and **c**) and from 100 plane (**d**).

previous calculations, especially the interlayer space (Sainz-Díaz et al. 2002). In this work, the application of the quantum mechanical methodology to crystal lattice models using pseudopotential linear-scaling DFT methods with numerical atomic orbitals, is extended to the study of pyrophyllite, the dehydroxylate derivatives, and the dehydroxylation process. In most cases we are able to obtain reasonably good agreement with experimental data with respect to the crystallographic and vibration properties of these derivatives. In this work, we present for the first time the intermediate dehydroxylation phase of pyrophyllite, the semidehydroxylate derivative. Other intermediates with water molecules in the interlayer space are also presented in this work and help with our discussion of the dehydroxylation process.

MODELS AND METHODS

Initial geometries were taken from X-ray diffraction data for the triclinic (1*Tc*) polymorph of pyrophyllite and its dehydroxylate derivative (Lee and Guggenheim 1981; Wardle and Brindley 1972). The experimental hydrogen positions were taken from previous studies (Giese 1979) after an optimization performed previously by us (Sainz-Díaz et al. 2001a). Several reaction intermediates, the semidehydroxylate, and intermediates with water molecules in the interlayer space, are studied in this work. The initial structure of the pyrophyllite semi-dehydroxylate model was taken from experimental data for pyrophyllite, including the position of the dehydroxylate AlOAl group from the pyrophyllite-dehydroxylate structure. In the semidehydroxylate and dehydroxylate derivatives with water molecules in the interlayer space, the water molecules were previously optimized before inclusion in the mineral structure, after which the hydrate complexes were fully optimized.

Total energy calculations were performed using the numerical atomic orbital (NAO) methodology implemented in the SIESTA program (Artacho et al. 1999; Sánchez-Portal et al. 1997). This is a method based on DFT and pseudo-potentials that scales linearly with the number of atoms in the simulation cell. The generalized gradient approximation (GGA) and the Perdew-Burke-Ernzerhof parameterization of the exchange-correlation functional were used. A uniform mesh with certain plane-wave cut-off energy is used to represent the electron density, the local part of the pseudopotential, and the Hartree and exchange-correlation potentials. Core electrons have been replaced by norm-conserving pseudopotentials (NCP) (Troullier and Martins 1991) factorized in the Kleinman-Bylander form (Kleinman and Bylander 1982). The pseudopotentials simulate the interaction between the valence electrons and the cores (nuclei plus core electrons) and neither core electrons nor core-wave functions have to be included explicitly. With this approximation, the valence-wave functions are substituted by pseudo-wave functions that do not present strong oscillations in the core region. The application of NCP to the study of 2:1 phyllosilicates is described elsewhere (Sainz-Díaz et al. 2002), yielding excellent results for the crystal structures of pyrophyllite, smectites, and illites. Recently, DFT calculations of pyrophyllite using ultrasoft pseudopotentials have been reported (Refson et al. 2003), but the agreement with experimental geometrical features was lower than those that obtained with our method.

The basis sets are composed of strictly localized numerical atomic orbitals (NAOs). Their localization cut-off radii correspond to an energy shift of 270 meV

TABLE 1. Experimental and calculated structural features of pyrophyllite and dehydroxylate and semidehydroxylate derivatives (lengths in Å and angles in degrees)

Sample	Pyrophyllite			Dehydroxylate		Semidehydroxylate
Basis set *	Exp†	DZP	DZPK‡	Exp	DZPK	DZPK
a	5.160(2)	5.16	5.25 (5.24)	5.19	5.32	5.28
b	8.966(3)	9.02	9.09 (9.09)	9.12	9.33	9.22
c	9.347(6)	9.16	9.32 (10.0)	9.50	9.53	9.36
α	91.18(4)	89.0	90.1 (90.0)	91.2	90.2	90.2
β	100.46(4)	101.5	100.8 (101.5)	100.2	99.0	100.2
γ	89.64(3)	90.0	89.9	88.6	88.8	89.6
Tetrahedral sheet thickness	2.15	2.17	2.23		2.20	2.21
Octahedral sheet thickness	2.08	2.13	2.14		2.33	2.22
Interlayer thickness	2.75		2.56		2.69	2.57
ΔZ§	0.24	0.31	0.28		0.39	0.42
τ ||	109.2	108.6	109.7		109.3	109.4
ψ #	57.0	56.7	56.5		61.9	54.5
Mean O-H	-	0.977	0.977			0.977
Mean Si-O **	1.62	1.67	1.67	1.62	1.67	1.67
Mean Al-O **	1.94	1.94	1.94	1.82	1.85	1.91
Mean Al-OH **	1.89	1.90	1.90	1.80	1.71	1.70
Al···Al			3.03		2.95, 3.41	3.00, 3.40
Si···Si			2.99, 3.13		3.03, 3.23	3.01, 3.14, 3.21

* Mesh cut-off energy of 150 Ry, DZP: Double zeta basis set with polarization function for all atoms except H atoms. DZPK is DZP with a sampling of four *k*-points.
† Experimental data from $(Si_{3.98}Al_{0.02})(Al_{1.97}Fe^{3+}_{0.03})O_{10}(OH)_2$ (Lee and Guggenheim 1981; Wardle and Brindley 1972).
‡ Values in brackets come from planewave DFT calculations (Refson et al. 2003).
§ Corrugation effect of basal surfaces.
|| τ is the O_{basal}-T-O_{apical} bond angle.
Octahedral flattening angle, ψ, cos ψ = O. th./2(M–O)].
** T is the cation of the tetrahedral sheet, M is the cation of the octahedral sheet.

(Artacho et al. 1999). The basis set used in this work is double-Z polarized (DZP) following the perturbative polarization scheme (Artacho et al. 1999). Calculations were restricted to certain values of *k*-points in the irreducible wedge of the Brillouin zone. This number was determined after preliminary calculations (see below). In all structures, all atoms and all cell parameters were relaxed by means of conjugated gradient minimizations.

Vibrational modes and frequencies were obtained from the force constant analysis calculated with the SIESTA program. The analysis of frequencies of the vibration modes was performed with the VIBRA program package (Soler et al. 2002).

The counterpoise correction (Boys and Bernardi 1970) was used in order to estimate the extent of basis set superposition error (BSSE) from the use of finite basis sets. The corrections usually give positive values, since superposition of two basis sets usually overestimates changes in energy. Thus, these corrections decrease the calculated energies. For reaction AB = A + B, five calculations are necessary to determine the energy of the AB structure: (1) optimization of AB, (2) total energy calculation of AB considering the atoms of part B as dummy atoms, (3) total energy calculation of AB considering the atoms of part A as dummy atoms, (4) total energy of the atoms of part A in the same positions that they are in AB, and (5) total energy of the atoms of part B in the same positions that they are in AB. The real energy of AB will be $E_{AB}' = E_{AB}$ + BSSE, the BSSE being determined by the equation BSSE = $(E_4 + E_5) - (E_2 + E_3)$

RESULTS AND DISCUSSION

Previous calculations with this methodology and these minerals found that the minimal conditions for accurate results should involve using the split-valence (double-zeta) basis set with polarization functions (DZP basis set), and at least 150 Ry of mesh cut-off energy (Sainz-Díaz et al. 2002). In the present work, different values of mesh cut-off energy and different numbers of *k*-points in the irreducible wedge of the Brillouin zone were explored, in order to optimize the level of the calculations. The higher the values of these parameters, the higher level of the calculations, but the computational effort is much greater. The total energy of the fully optimized crystalline structures was calculated with several values of mesh cut-off energy (from 150 to 400 Ry) and *k*-point number (from Γ point to 8 *k*-points). The best values for our samples were obtained with 400 Ry of cut-off energy and four *k*-points. The main geometrical features of the calculations for pyrophyllite (Fig. 1a) and the dehydroxylate derivative (Fig. 1b) are described in Table 1. Full optimizations with cut-off energies of 250, 350, and 400 Ry gave similar geometries to that obtained with 150 Ry. Optimizations with four *k*-points described the *c* parameter better than in previous calculations using only the Γ point, although similar geometrical features were yielded in all cases. A greater number of *k*-points does not yield a geometry closer to experimental results. Therefore, full optimizations of atomic positions and crystal lattice parameters were performed with mesh cut-off energy of 150 Ry and four *k*-points of the Brillouin zone. Final total energy of these optimized structures was calculated with 400 Ry of cut-off energy and four *k*-points sampling.

In pyrophyllite (Fig. 1a) our calculated lattice parameters reproduce the experimental values quite well (Table 1). The theoretical *a*, *b*, and *c* parameters match the experimental values. The experimental M-O and M-OH bond lengths (M = octahedral cation) are also reproduced in these calculations. The theoretical T-O bond length (T = tetrahedral cation) is slightly longer than the experimental values, a problem that has been traced to the perturbative polarization orbitals of T (Junquera et al. 2001). The differences of all parameters with respect to the experimental values is less than 2%. These results are consistent with recent calculations of pyrophyllite using pseudopotential planewave DFT methods (Bickmore et al. 2003). Nevertheless, our calculations better reproduce the interlayer space or *c* parameter [*c* = 9.32 Å (calculated) and 9.35 Å (experimental)] than previous studies [*c* = 9.84 Å (Bickmore et al. 2003), 10.0 Å (Refson et al. 2003), or 13.17 Å (Stackhouse et al. 2001)]. The existing interactions in the interlayer space of pyrophyllite are very weak and difficult to reproduce theoretically. Our calculations, based on NAO instead of plane-waves, yielded a good agreement between experimental and theoretical geometrical features, especially in the interlayer space.

In the dehydroxylate derivative (Fig. 1b) the calculated *c* parameter and the angles between unit-cell axes match the experimental values, although the calculated *a* and *b* parameters are slightly higher than the experimental values. The *a* and *b* parameters are smaller for pyrophyllite than for the dehydroxylate derivative due to the arrangement of the Al cations. The fivefold coordination of Al (^{V}Al) in the dehydroxylate derivative forms a trigonal bipyramid, where one O atom is bridging between two ^{V}Al atoms, with an Al-O bond length of 1.71 Å, which is shorter than that reported experimentally (Wardle and Brindley 1972). This is drastically shorter than the Al-OH bond length of pyrophyllite (1.90 Å), which explains the low value of the average Al-O bond length in the dehydroxylate (1.82 and 1.85 Å experimental and calculated values, respectively) with respect to those of pyrophyllite (1.94 Å). The Al-O-Al angle in the trigonal bipyramid is 180°, in agreement with the experimental data. A similar five-coordinate Al cation can be found in andalusite, but the Al-O-Al angle is 160° (Wardle and Brindley 1972). The higher value of the *c* parameter in the dehydroxylate is remarkable. This may be due to the fivefold coordination structure, which produces an increase of the tilting of the surrounding tetrahedra, also increasing the corrugation of the basal O atoms and the octahedral sheet thickness (Table 1). The cleavage of the OH groups makes the basal tetrahedral O atom, which is close to the ^{V}Al-O-^{V}Al bridging O atom, move to a position closer to this bridging O atom. Thus the deviation in *z* of this tetrahedral O atom from the rest of tetrahedral O atoms, that is the corrugation, increases. This is consistent with experimental observations (Wardle and Brindley 1972).

In this paper, we present the semidehydroxylate derivative as an intermediate phase in the dehydroxylation process of pyrophyllite. The semidehydroxylate derivative (Figs. 1c and 1d) has a crystal structure similar to that of pyrophyllite and the dehydroxylate, where half of the $Al(OH)_2Al$ groups are dehydroxylate alternating. Nevertheless, the *a*, *b*, and *c* parameters increase following the sequence: pyrophyllite < semidehydroxylate < dehydroxylate. The increase in lattice parameters might be due to an increasing number of five-coordinate Al atoms. This trigonal bipyramid results in a significant enlargement of the Al···Al distance (3.40 Å) with respect to pyrophyllite (3.03 Å) (Table 1). This enlargement is in the *a* and *b* directions. Similarly, dehydroxylation results in tilting of the surrounding tetrahedra, increasing the Si···Si distance (3.23 Å) with respect to pyrophyllite (3.13 Å).

The atomic positions are listed in Table 2, in which the calculated and experimental structures of pyrophyllite and the dehydroxylate derivative are compared. A good agreement is found between calculated and experimental values. Slight differences are found in the basal and hydroxyl O atoms of pyrophyllite, and in the Al atom and apical O atoms (O1 and O2) of the dehydroxylate derivative. The methodology presented in this work yields smaller differences between calculated and experimental values than recent pseudopotential planewave DFT calculations of pyrophyllite (Bickmore et al. 2003; Refson et al. 2003). The simulated powder X-ray diffraction patterns based upon the theoretical structure agree with the experimental patterns (Table 3) in terms of peak positions and relative intensities of the main reflections. The simulated diffraction patterns were obtained using diffraction software implemented within the Cerius2 package with an X-ray wavelength of 1.54 Å. The range of 5–60° 2θ was used for comparison (Fig. 2). No significant differences are found between the semidehydroxylate derivative and the pyrophyllite or dehydroxylate derivative. This could explain why this intermediate cannot be detected by means of XRD during the dehydroxylation process.

We can define some geometrical features in order to describe the OH geometry, such as the OH bond length, the orientation angle (ρ) of the OH bond with respect to the (001) plane, and the H···O non-bonding distances between the H atoms and the tetrahedral O atoms. Different H···O non-bonding distances can

TABLE 2. Atomic positions in the asymmetric unit (fractional coordinates in Å, based on the lattice parameters of Table 1) of the optimized crystal structures and experimental values (in brackets)*

Atom †	Pyrophyllite			Dehydroxylate		
	x	*y*	*z*	*x*	*y*	*z*
Al	0.4987	0.1676	0.0002	0.5291	0.1572	–0.0003
	(0.4995)	(0.1671)	(0.0000)	(0.552)	(0.149)	(0.000)
Si1	0.7505	–0.0067	0.2975	0.2216	0.4892	0.2978
	(0.7480)	(–0.0030)	(0.2917)	(0.225)	(0.486)	(0.286)
Si2	0.7675	0.3222	0.2994	0.7515	0.3131	0.2992
	(0.7595)	(0.3257)	(0.2923)	(0.749)	(0.312)	(0.286)
O1	0.65035	0.00129	0.11610	0.1057	0.5032	0.1232
	(0.6495)	(0.0018)	(0.1155)	(0.123)	(0.492)	(0.115)
O2	0.7356	0.3058	0.1171	0.7547	0.2853	0.1243
	(0.7314)	(0.3079)	(0.1158)	(0.728)	(0.292)	(0.115)
OH	0.2355	0.1973	0.1154	0.2500	0.2500	0.0000
	(0.2263)	(0.1927)	(0.1130)	(0.250)	(0.250)	(0.000)
Ob1	0.0679	0.3768	0.3703	0.0271	0.3844	0.3704
	(0.0550)	(0.3870)	(0.3589)	(0.037)	(0.378)	(0.355)
Ob2	0.7178	0.1592	0.3702	0.7215	0.1524	0.3712
	(0.7240)	(0.1637)	(0.3584)	(0.717)	(0.152))	(0.355)
Ob3	0.5653	0.4517	0.3393	0.5152	0.4218	0.3294
	(0.550)	(0.4480)	(0.3360)	(0.522)	(0.425)	(0.320)
H	0.1772	0.1196	0.1738			

* Wardle and Brindley (1972), Lee and Guggenheim (1981).
† Space group *C*, Ob is the basal O atom, OH in the dehydroxylate derivative is the bridging O atom of the five-coordinate Al.

TABLE 3. Main reflections from the powder XRD patterns of pyrophyllite and its dehydroxylate derivative

Reflection	Pyrophyllite				Dehydroxylate			
hkl	Exp*		Optimized		Exp*		Optimized	
	d (Å)	*I*	*d* (Å)	*I*	*d* (Å)	*I*	*d* (Å)	*I*
001	9.20	95	9.16	45	9.35	36	9.41	9
002	4.60	31	4.58	23	4.68	15	4.70	8
1$\bar{1}$0	4.42	11	4.49	6	4.50	7	4.62	5
110	4.42	90	4.48	100	4.42	100	4.54	100
11$\bar{1}$	4.26	64	4.32	74	4.34	42	4.39	44
111	4.23	19	4.31	24	4.24	31	4.32	21
021	4.05	81	4.08	87	4.13	36	4.18	48
02$\bar{1}$					4.08	9	4.18	4
112	3.49	16	3.50	15	3.54	10	3.55	8
022	3.18	36	3.22	42	3.24	12	3.31	16
003	3.07	82	3.05	80	3.12	60	3.13	54
11$\bar{2}$	2.95	26	2.97	27	3.01	11	3.09	15
13$\bar{1}$	2.55	23	2.58	26	2.61	7	2.65	7
201	2.57	11	2.61	15	2.58	10	2.64	7
200	2.54	22	2.57	26	2.55	10	2.62	4
13$\bar{1}$	2.41	30	2.45	30	2.47	15	2.54	14
131/202	2.41	48	2.45	45	2.440	14	2.47	14
133	2.08	14	2.09	19	2.126	14	2.13	12
134/312					1.663	16	1.70	14

Note: I = relative intensity.
* Wardle and Brindley (1972).

be defined: (1) that with the O atom that is in front of (H_{b1}) and where OH···O is contained in a plane perpendicular to (001) (this basal tetrahedral O atom will have the same *y* coordinate as the H atom); and (2) that with the apical O atoms of the tetrahedra that are in front of (H_{a1} and H_{a2}) (Fig. 3). More H···O non-bonding distances exist surrounding the H atom, but they are longer than the former ones and they are not significant.

The main geometrical features of the OH groups for the optimized crystal structures of pyrophyllite and the semidehydroxylate derivative are described in Table 4, including the orientation angle (ρ) of the O–H bond with respect to the (001) plane (Giese 1979), the OH bond length, and the main distances between the hydrogen and the surrounding tetrahedral O atoms. Both structures present similar values of *d*(OH) bond length and ρ(OH) angle. The calculated ρ(OH) value for pyrophyllite (33°) matches the experimental one (26–31.5°, Giese 1979) and is consistent with values from previous ab initio calculations (25.4°, Refson et al. 2003). The non-bonding H···O distances are longer in the semidehydroxylate than in pyrophyllite. This fact will have a direct consequence on the vibration frequencies of the OH groups (see below).

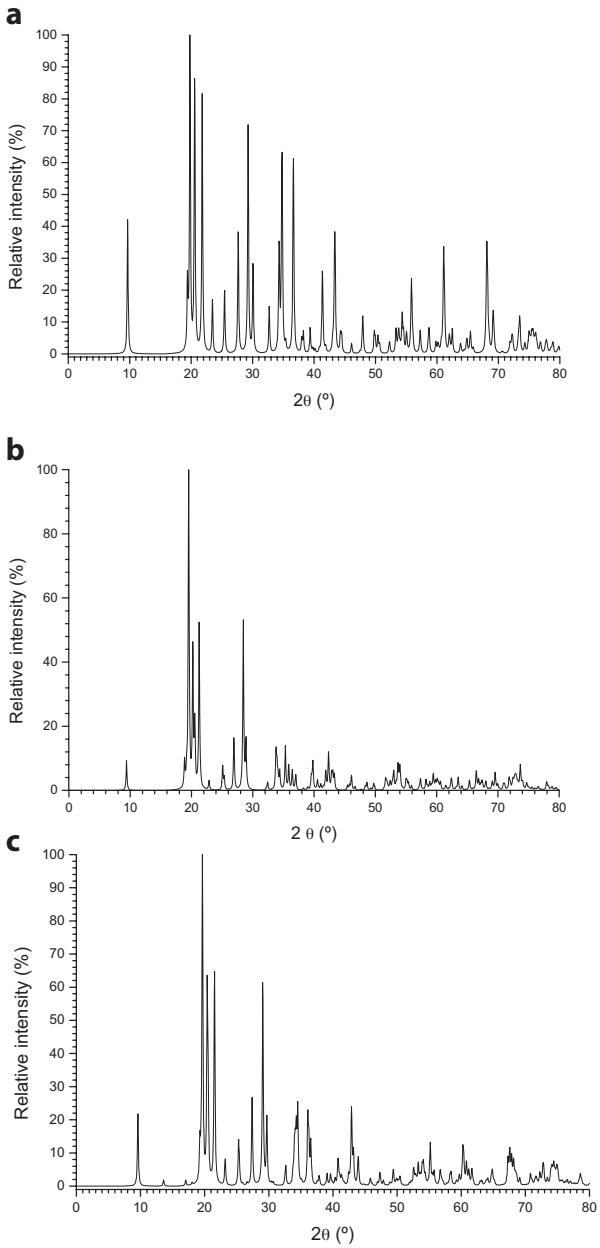

FIGURE 2. Simulated X-ray diffraction patterns of the optimized structures: pyrophyllite (**a**), dehydroxylate (**b**), and semidehydroxylate (**c**) derivatives.

Vibrations

The frequencies of the main vibration modes are described in Table 5. The ν(OH) vibration modes are not mixed with other modes. That means that only the O and H atoms of each OH group contribute to the normal coordinates of the ν(OH) vibration mode. In the δ(OH) and γ(OH) vibrations, the O and H atoms of each OH group are the main contributors to these vibration modes, but small contributions of displacements of other atoms are detected. In the rest of the vibration modes of these systems [ν(Si-O), ν(Al-O), etc.] the mixing of the displacement of other atoms is higher than in the former modes. The calculated ν(OH) frequency of pyrophyllite reproduces the experimental value (3675 cm^{-1}, Wang et al. 2002). The differences in the ν(OH)

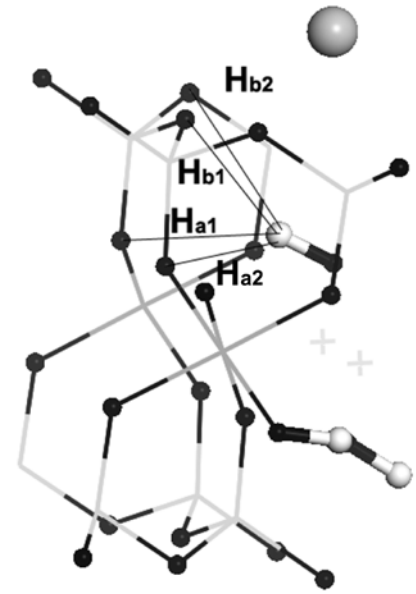

FIGURE 3. Non-bonding H···O distances between the H atom and the tetrahedral O atoms. White and black circles represent H and O atoms, respectively.

TABLE 4. Main geometrical features of the OH groups in the optimized crystal structures (distances in Å, and angles in degrees)

Structure	Pyrophyllite	Semidehydroxylate
d(OH)	0.977	0.977
ρ(OH)	33.0	35.0
H_{b1}	2.10	2.35
H_{a1}	2.76	3.15
H_{a2}	2.86	3.06

TABLE 5. Main calculated vibration frequencies (*s* and *as* means symmetric and asymmetric vibrations, respectively)

Vibration modes	Pyrophyllite	Dehydroxylate	Semidehydroxylate
ν(OH)	3655		3669, 3662
ν(Si-O)	1073-957	1113-940	1091 – 948
ν(^{V}Al-O)		1045, 1023*s*, 1013*as*	1027
ν(Si-O-Al)	969, 960, 893–818	1019*s*, 946*as*, 897*as*, 880*s*, 828*s*	1023, 1016, 891-808
ν(Si-O-VAl)		931, 840	
δ(OH)	951*s*, 948*as*, 921*as*		957*s*, 954*as*, 933*as*
γ(OH)	471*as*, 449*s*		517*s*, 493*as*

frequency between pyrophyllite and the semidehydroxylate intermediate are remarkable (14 cm^{-1} higher in the intermediate than in pyrophyllite). This is consistent with the experimental work of Wang et al. (2002), where the existence of one intermediate was detected during the dehydroxylation of pyrophyllite with a ν(OH) frequency 15 cm^{-1} higher than that in pyrophyllite. The OH bond lengths are identical in both pyrophyllite and semidehydroxylate. However, the larger non-bonding H···O distances in the semidehydroxylate indicate lower interactions between the H atom and the tetrahedral O atoms; hence the ν(OH) frequency will be higher than in pyrophyllite.

Symmetric and asymmetric vibrations were distinguished in δ(OH) and γ(OH) normal modes, whose frequencies are slightly higher in the semidehydroxylate intermediate than in pyrophyllite.

In the dehydroxylate derivative, the ν(^{V}Al-O) vibration mode, where ^{V}Al is the five-coordinate Al atom, is observed very clearly. However, it appears in the same zone as the ν(Si-O) vibrations. This makes this vibration mode very difficult to distinguish experimentally. Nevertheless, it is possible to determine it by calculation. This vibration is also detected in the semidehydroxylate intermediate. The ν(SiO-^{V}Al) vibration can be distinguished in the dehydroxylate derivative appearing in the same region as ν(SiO-^{VI}Al).

In pyrophyllite, the ν(Si-O) vibrations appear in the range 1073–957 cm^{-1}, according to the experimental values (1070–970 cm^{-1}, Farmer 1974). In the dehydroxylate derivative some ν(Si-O) and ν(SiO-Al) vibrations appear at frequencies slightly higher than in pyrophyllite, probably due to the higher tilting and distortion produced by the formation of the trigonal bipyramid of the five-coordinate Al atoms.

Dehydroxylation reaction

Many aspects of the dehydroxylation process of pyrophyllite are not well understood, such as the large temperature range (450–900 °C) where it occurs and the anomalous kinetic behavior (Bray and Redfern 2000; Wang et al. 2002). This process has been described previously as the reaction:

$$\text{pyrophyllite} \rightarrow \text{dehydroxylate derivative} + 2H_2O \quad (1)$$

The kinetic behavior of this process in pyrophyllite and other clay minerals is peculiar and the process can be also described as:

$$\text{pyrophyllite} \rightarrow \text{dehydroxylate}\cdot 2H_2O \rightarrow \text{dehydroxylate} + 2H_2O \quad (2)$$

where, in the first step of the reaction, two molecules of water per unit cell go to the interlayer space and the kinetics are highly dependant on the diffusion of the water molecules in the interlayer space.

Our starting hypothesis is that a semidehydroxylate derivative of pyrophyllite could be the real intermediate of the dehydroxylation process of pyrophyllite. We can describe the dehydroxylation process with the following reaction sequence:

$$\text{pyrophyllite} \rightarrow \text{semidehydroxylate} + H_2O \quad (3)$$

$$\text{semidehydroxylate} \rightarrow \text{dehydroxylate} + H_2O \quad (4)$$

For an energetic evaluation of these reactions, the water species should be calculated as a reaction product. Thus, a standard water molecule was included in the centre of a periodic cell with the same lattice parameters as pyrophyllite. The water molecule was fully optimized and the total energy was calculated with the same conditions as the previous crystal structures (E = –466.6967 eV).

Taking into account the total energy calculated for reactive and products (Table 6), the energy balance of Equation 1 will be:

$$\Delta E_1 = E_{\text{dehydroxylate}} + 2E_{\text{water}} - (E + \text{BSSE})_{\text{pyrophyllite}} = 1.2366 \text{ eV} = 28.53 \text{ kcal/mol}$$

This means that Equation 1 is endothermic, and pyrophyllite is more stable than the dehydroxylation products; hence high temperatures are necessary to activate the reaction. This fact justifies the rehydroxylation process of the dehydroxylate derivative, which in the presence of water goes to reactants, according to experimental observation.

Analogously, the energy balance of Reaction 3 will be:

$$\Delta E_3 = (E + \text{BSSE})_{\text{semidehydroxylate}} + E_{\text{water}} - (E + \text{BSSE})_{\text{pyrophyllite}} = 0.8102 \text{ eV} = 18.68 \text{ kcal/mol}$$

Hence the reaction energy to form the semidehydroxylate intermediate during the dehydroxylation of pyrophyllite is much lower than in Reaction 1, requiring a lower temperature to produce this intermediate than for the complete dehydroxylation reaction. This fact confirms that the previously unknown intermediate phase (Wang et al. 2002) is likely the semidehydroxylate derivative.

For the dehydroxylation of the semidehydroxylate derivative (Reaction 4), the energy balance of the total reaction is $\Delta E_4 = \Delta E_1 - \Delta E_3 = 9.83$ kcal/mol. Hence the semidehydroxylate intermediate is more stable than the dehydroxylate product

TABLE 6. Total energy and crystal lattice parameters (distances in Å and angles in degrees) for the optimized structures*

Compound	Energy†	*a*	*b*	*c*	α	β	γ
pyrophyllite	–11642.4845	5.25	9.09	9.32	90.1	100.8	90
semidehydroxylate	–11173.0758	5.28	9.22	9.36	90.2	100.2	89.6
semidehydroxylate·H_2O	–11640.3782	5.22	9.39	9.54	92.5	100.0	87.6
dehydroxylate·$2H_2O$	–11638.9548	5.29	9.21	9.36	90.1	98.3	90.2
dehydroxylate·H_2O	–11171.3042	5.33	9.24	9.39	90.2	99.9	89.5
dehydroxylate	–10703.8765	5.32	9.33	9.53	90.2	99.0	88.8

* Optimized with energy cut-off = 150 Ry and four *k*-point sampling.
† In eV, calculated with energy cut-off = 400 Ry and four *k*-point sampling for the optimized structure.

and higher temperatures will be necessary to complete the dehydroxylation process. This is consistent with experimental work, where the intermediate was detected at 650 °C and it was necessary to increase the temperature to 900 °C to complete the dehydroxylation (Wang et al. 2002). The greater stability of the semidehydroxylate explains the experimental observation of spontaneous rehydroxylation of the dehydroxylate derivative in the presence of water, where extra IR signals were observed during this process and these signals appeared at frequencies similar to the ν(OH) of the semidehydroxylate derivative (Heller at al. 1962; Wang et al. 2002).

Our results agree with experimental fact where the dehydroxylation of pyrophyllite involves two endothermic processes with a loss of water in two steps (Wang et al. 2002). This fact, the spectroscopic results, and our calculations conclude that an intermediate is formed during the thermically induced dehydroxylation of pyrophyllite; we find that the semidehydroxylate derivative is the real intermediate. This conclusion does not agree with the previous assumption that the mechanism of the pyrophyllite dehydroxylation is a combination of dehydroxylation and rehydroxylation (Wang et al. 2002). However, our conclusion is consistent with the experimental assumption that there is a kinetic control during the process in both steps for the release of the water molecules along the interlayer space. The release kinetics are highly dependent on the thermal conditions (e.g., heating rate) and the particle size.

In the next step, we considered that the water release should be taken into account in both steps of our mechanism, the formation of the semidehydroxylate and the dehydroxylation of this intermediate. We have calculated and optimized the crystal structure of the different possible intermediates defined in the reactions shown above (Table 6). The intermediates with water molecules in the interlayer space show a crystal lattice that is similar to the derivatives without these water molecules. The *b*, *c*, and α parameters are higher and γ is smaller in the semidehydroxylate with a water molecule than in the semidehydroxylate derivative without water.

In the dehydroxylate·$2H_2O$ (Fig. 4a), the semidehydroxylate·H_2O (Figs. 4b and 4c), and the dehydroxylate·H_2O (Fig. 5), the water molecules are stabilized in the interlayer space by hydrogen bonds between the hydrogen atoms and the tetrahedral O atoms. However, in dehydroxylate·$2H_2O$, the water molecules are inside the hexagonal cavity of tetrahedra, with a weak coordination between the O atom of water and Al cations [*d*(O···Al) = 2.4 Å] and an ^{V}Al-O-^{V}Al angle of 124.1°, which is far from the 180° seen in the dehydroxylate structure. A similar structure was found in the dehydroxylate·H_2O intermediate. The interlayer space is too small to accommodate these water molecules. In contrast, in the semidehydroxylate·H_2O, the water molecules are in the interlayer space with a strong hydrogen bond with a basal tetrahedral O atom [*d*(O···H) = 1.7 Å] and with an electrostatic interaction with an Si atom [*d*(O···Si) = 1.98 Å] (Fig. 4c).

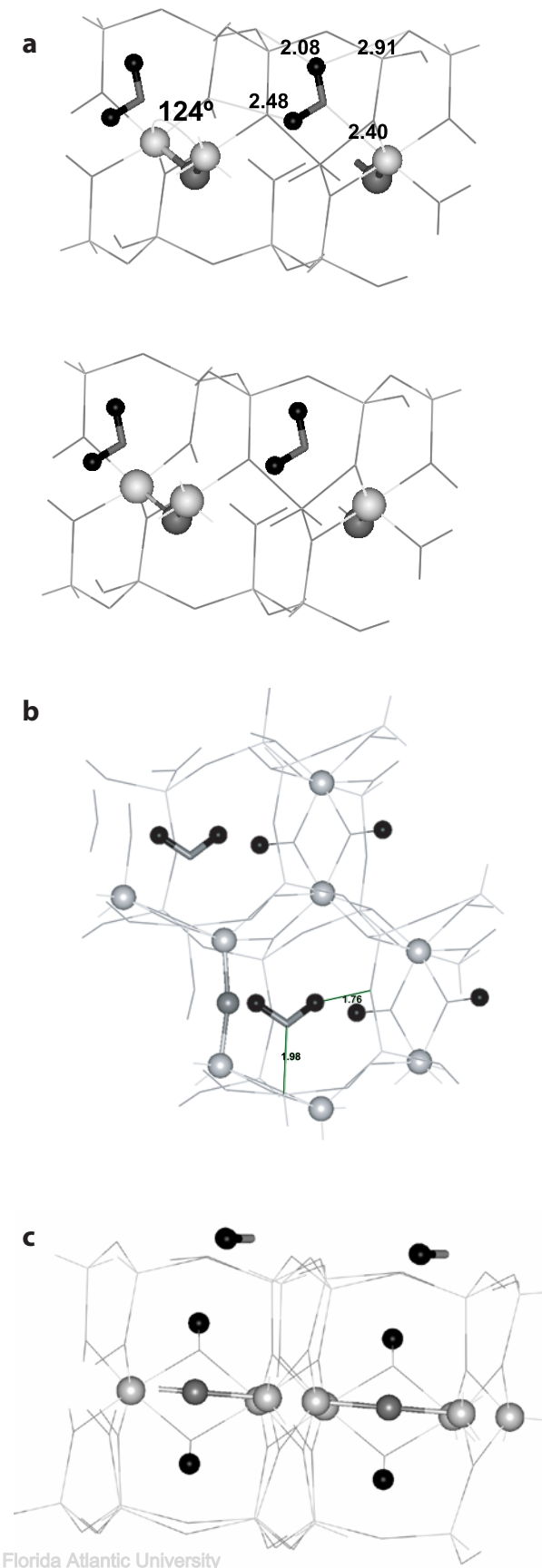

FIGURE 4. Possible intermediates of the dehydroxylation process of pyrophyllite: dehydroxylate·$2H_2O$ (**a**) and semihydroxylate·H_2O projected on the 001 (**b**) and 010 (**c**) planes. The H atoms, the O of the OH groups, and the ^{V}Al-O-^{V}Al groups are shown as black, dark grey, and light grey spheres, respectively.

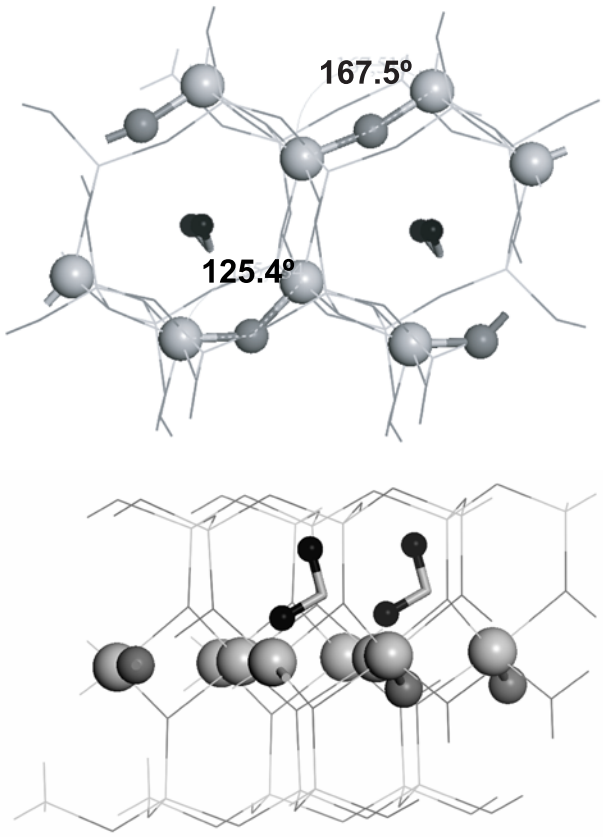

FIGURE 5. Crystal structure of the dehydroxylate·H_2O intermediate in the dehydroxylation process of pyrophyllite, viewed from the 001 (**a**) and 010 (**b**) planes. The H atoms, the O of the OH groups, and the ^{V}Al-O-^{V}Al groups are shown as black, dark grey, and light grey spheres, respectively.

Considering the second part of Reaction 2, we calculated the total energy of the reaction species. Hence, the energy balance of this reaction will be:

$$\Delta E_{2b} = E_{\text{dehydroxylate}} + 2E_{\text{water}} - (E + \text{BSSE})_{\text{dehydroxylate·2H2O}} = -0.8599 \text{ eV} = -19.83 \text{ kcal/mol}$$

This reaction is exothermic. The high energy of the dehydroxylate·$2H_2O$ intermediate is due to the repulsion between O atoms that neutralizes the strong hydrogen bonds between the water H atoms and the tetrahedral O atoms. The water O atom forces the ^{V}Al-O-^{V}Al bridge-bond to bend away from the 180° that it has in the final dehydroxylate product (Fig. 4a). Therefore, the release of water from the interlayer space is thermodynamically favored and is controlled kinetically.

Taking into account the energy balances of Reaction 1 and the second part of Reaction 2, the energy balance of the first part of this reaction will be $\Delta E_{2a} = \Delta E_1 - \Delta E_{2b} = 48.36$ kcal/mol. Hence, the dehydroxylate·$2H_2O$ can be an intermediate phase of high energy where a high temperature is necessary for its formation and after which it spontaneously yields the dehydroxylate product, following the scheme of Figure 6a.

Considering the formation of the semidehydroxylate intermediate, we can obtain the following reaction (pyro = pyrophyllite), whose energy balance is described in Figure 6a:

$$\text{pyro} \rightarrow \text{semidehydroxylate·}H_2O \rightarrow \text{dehydroxylate·}2H_2O \rightarrow \text{dehydroxylate} + 2H_2O \quad (5)$$

With a slow heating rate or a very small particle size, the release of water from the interlayer space can finish before the cleavage of the second water molecule and the following reactions can be also considered:

$$\text{semidehydroxylate·}H_2O \rightarrow \text{semidehydroxylate} + H_2O \quad (6)$$

$$\text{semidehydroxylate} \rightarrow \text{dehydroxylate·}H_2O \rightarrow \text{dehydroxylate} + H_2O \quad (7)$$

In this case the semidehydroxylate derivative will be also the main intermediate of the dehydroxylation process, along with two high-energy intermediates: the semidehydroxylate and dehydroxylate structures, both with one water molecule per unit cell in the interlayer space, respectively. Therefore, the energy profile of this mechanism will be that described in Figure 6b.

In both cases the semidehydroxylate derivative is the main intermediate in the dehydroxylation of pyrophyllite independently of the mechanism for water release. This fact confirms the experimental spectroscopic result found during this process, identifying the previously unknown intermediate phase. The energy profile of the reaction is consistent with the rehydroxylation possibility and the wide temperature range of the dehydroxylation process found experimentally. Work is in preparation to study the mechanism and transition states for each step of these reactions.

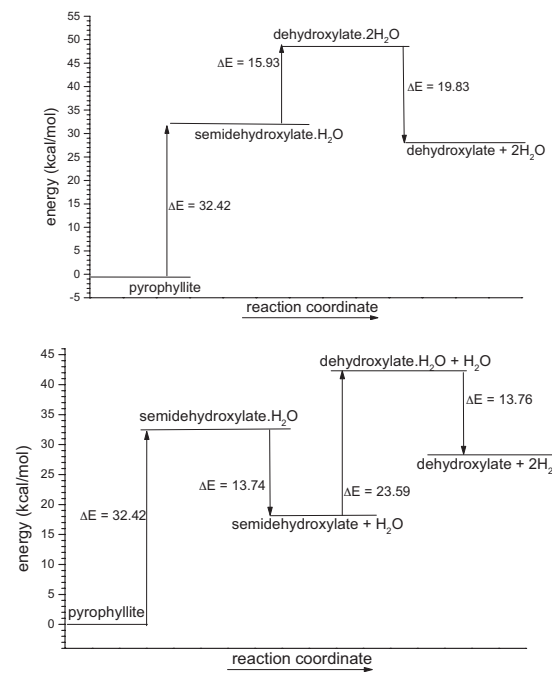

FIGURE 6. Energy profiles (in kcal/mol) of the dehydroxylation reaction in pyrophyllite.

ACKNOWLEDGMENTS

Authors are thankful to E. Artacho for fruitful discussions and for allowing us to use the SIESTA program, and also to the "Centro Técnico de Informática" of CSIC and the "Centro de Supercomputación de la Universidad de Granada" for allowing the use of his computational facilities. E. Escamilla-Roa is thankful to AECI for financial support. This work was supported by grants from the Spanish MCYT and the European FEDER funds.

REFERENCES CITED

Artacho, E., Sánchez-Portal, D., Ordejón, P., García, A., and Soler, J.M. (1999) Linear-scaling ab-initio calculations for large and complex systems. Physic Status Solidi, 215, 809–817.

Bickmore, B.R., Rosso, K.M., Nagy, K.L., Cygan, R.T., and Tadanier, C.J. (2003) Ab initio determination of edge surface structures for dioctahedral 2:1 phyllosilicates: Implications for acid-base reactivity. Clays and Clay Minerals, 51, 359–371.

Botella, V., Timón, V., Hernández-Laguna, A., and Sainz-Díaz, C.I. (2004) Hydrogen bonding and vibrational properties of hydroxy groups in the crystal lattice of dioctahedral clay minerals by means of First Principles calculations. Physics and Chemistry of Minerals, in press.

Boys, S.F. and Bernardi, F. (1970) The calculation of small molecular interactions by the differences of separate total energies. Some procedures with reduced errors. Molecular Physics, 19, 553–566.

Bray, H.J. and Redfern, S.A.T. (2000) Influence of counterion species on the dehydroxylation of Ca^{2+}-, Mg^{2+}-, Na^{+}-, and K^{+}-exchanged Wyoming montmorillonite. Mineralogical Magazine, 64, 337–346.

Bridgeman, C.H., Buckingham, A.D., Skipper, N.T., and Payne, M.C. (1996) Ab initio total energy study of uncharged 2:1 clays and their interaction with water. Molecular Physics, 89, 879–888.

Drits, V.A., Besson, G., and Muller, F. (1995) An improved model for structural transformation of heat-treated aluminous dioctahedral 2:1 layer silicates. Clay and Clay Minerals, 43, 718–731.

Emmerich, K., Madsen, F.T., and Kahr, G. (1999) Dehydroxylation behavior of heat-treated and steam-treated homoionic cis-vacant montmorillonites. Clays and Clay Minerals, 47, 591–604.

Farmer, V.C. (1974) The layer silicates. In V.C. Farmer, Ed., The infrared spectra of minerals, p. 331–363. Mineralogical Society, London.

Fitzgerald, J.J., Hamza, A.I., Dec, S.F., and Bronnimann, C.E. (1996) Solid-state silicon-29 and aluminium-27 nuclear magnetic resonance investigation of the dehydroxylation of pyrophyllite. Journal of Physical Chemistry, 88, 6206–6209.

Giese, R.F. (1979) Hydroxyl orientations in 2:1 phyllosilicates. Clays and Clay Minerals, 27, 213–223.

Guggenheim, S., Chang, Y.-H., Koster van Gross, A.F. (1987) Muscovite dehydroxylation: high-temperature studies. american Mineralogist, 72, 537–550.

Heller, L., Farmer, V.C., Mackenzie, R.C., Mitchell, B.D., and Taylor, H.F.W. (1962) The dehydroxylation and rehydroxylation of triphormic dioctahedral clay minerals. Clay Minerals Bulletin, 5, 56–72.

Hobbs, J.D., Cygan, R.T., Nagy, K.L., Schultz, P.A., and Sears, M.P. (1997) All-atom ab initio energy minimization of the kaolinite crystal structure. American Mineralogist, 82, 657–662.

Junquera, J., Paz, O., Sánchez-Portal, D., and Artacho, E. (2001) Numerical atomic orbitals for linear-scaling calculations. Physics Reviews B, 64, 235111.

Kleinman, L. and Bylander, D.M. (1982) Efficacious form for model pseudopotentials. Physics Reviews Letters, 48, 1425–1428.

Lee, J.H. and Guggenheim, S. (1981) Single crystal X-ray refinement of pyrophyllite-1*Tc*, American Mineralogist, 66, 350–357.

Refson, K., Park, S-H., and Sposito, G. (2003) Ab initio computational crystallographic of 2:1 clay minerals: 1. Pyrophyllite-1Tc. Journal of Physical Chemistry B, 107, 13376–13383.

Sainz-Díaz, C.I., Timón, V., Botella, V., and Hernández-Laguna, A. (2000) Isomorphous substitution effect on the vibration frequencies of hydroxyl groups in molecular cluster models of the clay octahedral sheet. American Mineralogist, 85, 1038–1045.

Sainz-Díaz, C.I., Hernández-Laguna, A., and Dove, M.T. (2001a) Modelling of dioctahedral 2:1 phyllosilicates by means of transferable empirical potentials. Physics and Chemistry of Minerals, 28, 130–141.

———(2001b) Theoretical modelling of cis-vacant and trans-vacant configurations in the octahedral sheet of illites and smectites. Physics Chemistry of Minerals, 28, 322–331.

Sainz-Díaz, C.I., Timón, V., Botella, V., Artacho, E., and Hernández-Laguna, A. (2002) Quantum mechanical calculations of dioctahedral 2:1 phyllosilicates: Effect of octahedral cation distribution in pyrophyllite, illite, and smectite. American Mineralogist, 87, 958–965.

Sánchez-Portal, D., Ordejón, P., Artacho, E., and Soler, J.M. (1997) Density-functional method for very large systems with LCAO basis sets. International Journal of Quantum Chemistry, 65, 453–461.

Soler, J.M., Artacho, E., Gale, J.D., García, A., Junquera, J., Ordejón, P., and Sánchez-Portal, D. (2002) The Siesta method for ab initio order-N materials simulation. Journal of Physics Condensded Matter, 14, 2745–2758.

Stackhouse, S., Coveney, P.V., and Sandre E. (2001) Plane-wave density functional theoretic study of formation of clay-polymer nanocomposite materials by self-catalyzed in situ intercalate polymerization. Journal of American Chemical Society, 123, 11764–11774.

Teppen, B.J., Rasmussen, K., Bertsch, P.M., Miller, D.M., and Schafer, L. (1997) Molecular dynamics modelling of clay minerals. 1. Gibbsite, kaolinite, pyrophyllite, and beidellite. Journal of Physical Chemistry B, 101, 1579–1587.

Timón, V., Sainz-Díaz, C.I., Botella, V., and Hernández-Laguna, A. (2003) Isomorphous cation substitution in dioctahedral 2:1 phyllosilicates by means of ab initio quantum mechanical calculations on clusters. American Mineralogist, 88, 1788–1795.

Troullier, N. and Martins, J.L. (1991) Efficient pseudopotentials in spin-density functional calculations. Physical Reviews B, 43, 1993–2000.

Wang, L., Zhang, M., Redfern, S.A.T., and Zhang, Z. (2002) Dehydroxylation and transformation of the 2:1 phyllosilicate pyrophyllite at elevated temperatures: an infrared spectroscopic study. Clays and Clay Minerals, 50, 272–283.

Wardle, R. and Brindley, G.W. (1972) The crystal structures of pyrophyllite, 1Tc, and its dehydroxylate. American Mineralogist, 57, 732–750.

MANUSCRIPT RECEIVED SEPTEMBER 6, 2003
MANUSCRIPT ACCEPTED FEBRUARY 2, 2004
MANUSCRIPT HANDLED BY JAMES KUBICKI